Green Chemical Engineering xxx (xxxx) xxx

Contents lists available at ScienceDirect

Green Chemical Engineering

journal homepage: www.keaipublishing.com/en/journals/green-chemical-engineering

Original Article

Regulated CO adsorption by the electrode with OH^- repulsive property for enhancing C–C coupling

Qixing Zhang [a], Dan Ren [b], Jing Gao [b], Zhongke Wang [a], Juan Wang [a], Sanjiang Pan [a], Manjing Wang [a], Jingshan Luo [a], Ying Zhao [a], Michael Grätzel [b], Xiaodan Zhang [a,*]

[a] Institute of Photoelectronic Thin Film Devices and Technology, Key Laboratory of Photoelectronic Thin Film Devices and Technology of Tianjin, Ministry of Education Engineering Research Center of Thin Film Photoelectronic Technology, Renewable Energy Conversion and Storage Center, Nankai University, Solar Energy Conversion Center, Nankai University, Tianjin, 300350, China

[b] Laboratory of Photonics and Interfaces, Institute of Chemical Sciences and Engineering, École Polytechnique Fédérale de Lausanne (EPFL), 1015, Lausanne, Switzerland

HIGHLIGHTS

- The introduction of polymer for designing the Cu electrode leads to improved selectivity of C_{2+} products.
- Enhanced FE ratio of the C_{2+} products-to-CH_4 from 0.5 on Cu mesh to 11.2 on Cu mesh/Nafion.
- The negative background charge of Nafion polymer produces an exclusion to OH^-, contributing to reducing part of OH^- and increasing CO adsorbed on active sites, and enhancing C–C coupling.
- Both Cu foil/Nafion and Cu foam/Nafion were also prepared, and the FE ratio of the C_{2+} products-to-CH_4 is 2.9 and 7.3, respectively.

GRAPHICAL ABSTRACT

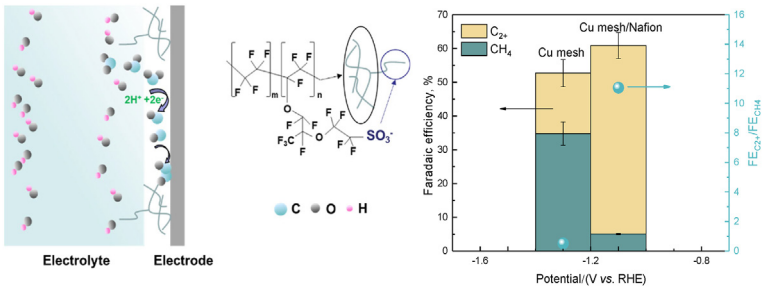

ARTICLE INFO

Keywords:
CO_2 reduction
Polymer modified copper electrode
Repulsive to OH^-
Regulated CO adsorption
Enhancing C–C coupling

ABSTRACT

Electrochemical CO_2 reduction driven by renewable electricity is one of the promising strategies to store sustainable energy as fuels. However, the selectivity of value-added multi-carbon products remains poor for further application of this process. Here, we regulate CO adsorption by forming a Nafion layer on the copper (Cu) electrode that is repulsive to OH^-, contributing to enhanced selectivity of CO_2 reduction to C_{2+} products with the suppression of C_1 products. The *operando* Raman spectroscopy indicates that the local OH^- would adsorb on part of active sites and decrease the adsorption of CO. Therefore, the electrode with repulsive to OH^- can adjust the concentration of OH^-, leading to the increased adsorption of CO and enhanced C–C coupling. This work shows that electrode design could be an effective strategy for improving the selectivity of CO_2 reduction to multi-carbon products.

* Corresponding author.
E-mail address: xdzhang@nankai.edu.cn (X. Zhang).

https://doi.org/10.1016/j.gce.2022.07.007
Received 2 May 2022; Received in revised form 29 June 2022; Accepted 19 July 2022
Available online xxxx

Please cite this article as: Q. Zhang et al., Regulated CO adsorption by the electrode with OH^- repulsive property for enhancing C–C coupling, Green Chemical Engineering, https://doi.org/10.1016/j.gce.2022.07.007

1. Introduction

Electrochemical reduction of carbon dioxide (CO_2) promises a key technology in coming years to valorize CO_2 to value-added chemicals [1,2]. Copper (Cu), as a unique metal, is capable of catalyzing the production of hydrocarbons and oxygenates in the electrochemical reduction of CO_2 [3–6]. However, achieving high selectivity toward multi-carbon products, widely used as fuels or feedstock chemicals in industry, remains a significant challenge [7,8].

Recently, facets [9,10] and grain boundary design [11–14], nanostructure engineering [15–17], alloy [18,19], electrolyte engineering [20,21], and interface design [22,23] were implemented as effective strategies to modify the selectivity of Cu. There are correlated scaling relations for the binding strengths of different intermediates, which means that one adsorbed species changed by optimizing the electronic structure of Cu will affect another species from being optimal [24,25]. Adjusting the microenvironment around the electrode can change the selectivity without changing the electronic structure of Cu.

For example, Wakerley et al. [26] and Niu et al. [27] in their respective work reported that constructing a hydrophobic interface could trap CO_2 on the surface of the Cu electrode, promoting the performance of C–C coupling. Xing et al. [28] and Liang et al. [29] modified a Cu with hydrophobic poly tetra fluoroethylene (PTFE) or polyvinylidene fluoride (PVDF), respectively. A hydrophobic catalyst microenvironment with high local pH was created, leading to improved selectivity of multi-carbon products. Improving hydrophobicity of interface helps to increase the concentration of CO_2 or CO intermediate and local pH, leading to enhanced CO_2 reduction to multiple carbonaceous products by suppressing H_2 and C_1 products [30–34].

As we know, the depletion of proton leads to more OH^-, or in other words, increased pH [35]. More OH^- near the electrode will cover part of the active sites of the electrode surface, leading to decreasing selectivity of C–C coupling [36]. Therefore, we use the Nafion with the repulsion of OH^- characteristic to optimize the local concentration of OH^- on the active sites. Cu mesh/Nafion electrode showed enhanced selectivity and partial current density for the formation of multi-carbon products, with the simultaneous suppression of methane (CH_4). The Faradaic efficiency (FE) ratio of C_{2+}/CH_4 on Cu mesh/Nafion increased significantly compared to Cu mesh without modification. *Operando* Raman spectroscopy demonstrated that the improved performance of Cu mesh/Nafion is attributed to the decreased OH adsorption by the repulsion of Nafion to OH^-, contributing to more CO adsorbed on active sites and enhanced C–C coupling. This work provides a promising strategy for constructing an effective electrode for enhancing the selectivity of multi-carbon products.

2. Experimental details

2.1. Chemicals

Potassium bicarbonate ($KHCO_3$, $\geq$ 99.95%, Sigma-Aldrich), hydrochloric acid (HCl, analysis pure), Nafion (510211-25 ML, Sigma-Aldrich), PVDF (XIYA), 1-methyl-2-pyrrolidinone (NMP) (99.5%, Macklin), Cu mesh (99.99%, 100 mesh), Cu foam, and Cu foil (99.99%) were purchased from Hebei Zhanmo metal materials. The chemical reagents were not further purified in use. The solutions used in the tests were all deionized water with 18.2 MΩ cm.

2.2. Electrodes preparation

Cu mesh. All the Cu mesh electrodes were cleaned in dilute hydrochloric acid and deionized water, then dry with a nitrogen gun.

Cu mesh/Nafion. The cleaned Cu mesh was put into a vessel containing Nafion solution, soak it for 4 min, taken it out, and let stand in the air for 24 h at room temperature to dry.

Cu mesh/PVDF. 250 mg PVDF was mixed with 4.7 mL NMP, then the ultrasonic dispersion for 1 h. The cleaned Cu mesh was put into a vessel containing the mixed solution, soak it for 4 min, taken it out, and let stand in the air for 48 h at room temperature to dry.

Cu foam and Cu foil. It is consistent with the preparation process of Cu mesh.

Cu foam/Nafion and Cu foil/Nafion. It is consistent with the preparation process of Cu mesh/Nafion.

2.3. Material characterization

X-ray diffraction (XRD) (Rigaku) with Cu K_α radiation was devoted to the analysis of the crystal structural characterization. Apreo S LoVac microscope was used to measure the surface morphology. JEM-2800 with a field emission gun operated at 200 kV was used for acquired transmission electron microscope (TEM) images. X-ray photoelectron spectroscopy (XPS) spectrum was achieved by Thermo Scientific ESCALAB 250Xi with an Al K_α source.

***Operando* Raman spectroscopy.** *Operando* Raman spectroscopy was achieved by the Horiba XPloRA confocal Raman microscope with a water immersion objective (100 ×, Olympus). A 638 nm wavelength laser is used. We use a three-electrode system for testing in a CO_2-saturated 0.1 M $KHCO_3$ solution. IrO_2 counter electrode was prepared by electrodeposited and Ag/AgCl as the reference electrode. A Teflon FEP parafilm (Dupon, 25 μm thickness) was used to cover the objective with a water drop between parafilm and objective.

Electrocatalytic measurements. Autolab Pgstat204 was used for electrochemical tests. All the electrocatalytic measurements were carried out in a three-electrode system. The reference electrode and counter electrode is Ag/AgCl and IrO_2/Ti, respectively. There are two compartments in the H-type cell by an anion exchange membrane under ambient conditions. 0.1 M $KHCO_3$ solution was used as the electrolyte, and CO_2 gas was flowed into the electrolyte continuously by a mass flow controller at a specified flow rate of 10 mL min^{-1}, and stirred at a rate of 1500 r min^{-1} during electrolysis. All the applied potentials were IR-compensated and converted to the RHE scale.

During electrolysis, gas-phase products from the H-cell were quantified by a gas chromatograph (Thermo scientific, Trace 1310) equipped with N_2 as the carrier gas. Gas chromatography (GC) is composed of Porapak N column and MoleSieve 5A column, one thermal conductivity detector (TCD), and two flame ionization detector (FID) detectors. Solution phase products were analyzed using high performance liquid chromatography (HPLC) (Agilent 1260 Infinity II) with 0.5 mM H_2SO_4 as the carrier liquid. HPLC contains a BIO-RAD column (Aminex, HPX-87H), VWD, and FID detector. Typically, 900 μL of the post-electrolysis catholyte was mixed with 100 μL of 4.5 M H_2SO_4 as the acidizing fluid.

Electrochemically active surface area (ECSA) measurement. The double-layer capacitance was measured for quantifying the ECSA of the samples. The non-faradaic current densities are linearly related to scanning rates, the slope of this curve was the double-layer capacitance. Firstly, we carried out the cyclic voltammetry (CV) measurements at scan rates of 20, 40, 60, 80, and 100 mV s^{-1} and the potential range is the non-faradaic window (Figs. S7, S11, and S12). The rough factors were obtained by the following equation: $RF = C_{DL}/C_S$, where specific capacitance C_S = 0.03 mF cm^{-2} [37].

2.4. Calculation of the turnover efficiency (TOF)

The production rate of CO gas as $TOF_{CO(g)}$, CO was further reduced to multi-carbon products as TOF_{*CO}, and CO was further reduced to CH_4 as TOF_{CH4}.

Therefore, the value of TOF_{*CO} can be achieved by:

$$TOF_{*CO} = 2TOF_{C2H4} + 2TOF_{C2H6} + 2TOF_{CH3COOH} + 2TOF_{C2H5OH} + 3TOF_{C3H6O} + 3TOF_{C3H8O} + 3TOF_{C3H7OH}$$

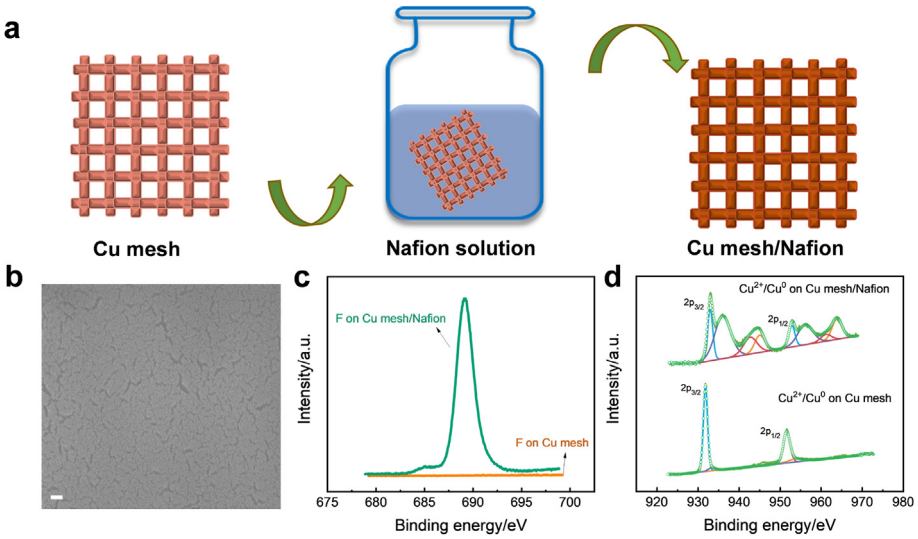

Fig. 1. Preparation and characterization of Cu mesh/Nafion. (a) Schematic of the process of synthesizing Cu mesh/Nafion electrodes. (b) SEM image of Cu mesh/Nafion, Scale bar: 100 nm. (c~d) High-resolution F 1s and Cu 2p XPS spectra of Cu mesh and Cu mesh/Nafion samples.

In the case of the CO products, the equation of TOF_{CO} was calculated by:

$$TOF_{CO} = \frac{j_{specific}}{nF}$$

Where F is the Faradaic constant, and n is the transfer electron number. $j_{specific}$ is the specific partial current density.

3. Results and discussion

3.1. Synthesis and characterization of electrodes

We prepared Cu mesh electrodes (100 mesh) covered with a layer of Nafion film. Cu mesh was dipped in 5 wt% Nafion solution for 4 min firstly, followed by drying in air at ambient temperature for about 24 h to form Cu mesh/Nafion (Fig. 1a). Compared to the surface of Cu mesh (Fig. S1a), the surface of Cu mesh/Nafion electrode shows a thin film with a crack structure (Fig. 1b). The thickness of Nafion film is about 4.9 μm, as shown in the cross-sectional image (Fig. S2a). EDS mapping of F and Cu elements demonstrates that the Cu surface is covered with Nafion film (Fig. S2b and S2cc).

X-ray photoelectron spectroscopy (XPS) was conducted to investigate the Nafion film and the oxidation state of Cu (Fig. 1c and d). On Cu mesh/Nafion sample, the peak at 688.2 eV represents F 1s, which also verifies that the Nafion is covered on the surface of the Cu mesh (Fig. 1c) [37]. Compared to Cu mesh, the peaks at 936 and 956 eV corresponding to Cu^{2+} oxidation states become more obvious on Cu mesh/Nafion (Fig. 1d) [38,39], which is attributed to the quick oxidation of the surface when covered with Nafion and dried in the air [40,41].

After CO_2 reduction, the surfaces of Cu mesh and Cu mesh/Nafion were also characterized by SEM (Figs. S1b and S3), which shows no noticeable difference compared with the surface before reduction. Besides, the XPS peak of F 1s on Cu mesh/Nafion also has a similar position before and after reduction (Fig. S4a), indicating that Nafion species remain on Cu mesh. After CO_2 reduction, the Cu^{2+} oxidation states almost disappear (Fig. S4b) due to the long-term reduction reaction [42].

3.2. Enhanced performance of CO_2 reduction

The electrochemical CO_2 reduction reaction (CO_2RR) was evaluated on Cu mesh and Cu mesh/Nafion electrodes in an H-type electrochemical cell under potentiostatic measurements from −1.0 V to −1.25 V *vs.* RHE with CO_2-saturated 0.1 M $KHCO_3$ as the electrolyte (Figs. S5 and S6). The gas and liquid products were quantified by online GC and HPLC, respectively.

The geometric current density for overall reaction and CO_2 reduction as a function of applied potential is shown in Fig. S7 and Tables S1 and S2. Both j_{total} and j_{CO2RR} on Cu mesh/Nafion are improved as compared

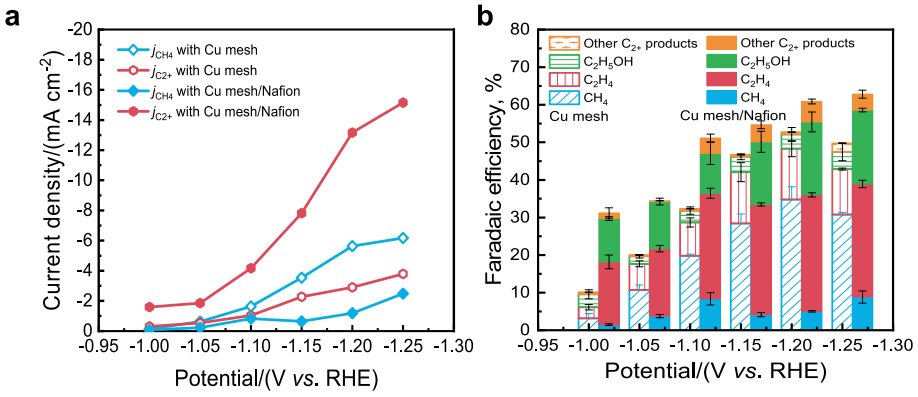

Fig. 2. CO_2RR performance on Cu mesh and Cu mesh/Nafion. (a) The partial current density of CH_4 (j_{CH4}) and C_{2+} products (j_{C2+}) on Cu mesh and Cu mesh/Nafion. (b) Faradaic efficiency of CH_4, C_2H_4, C_2H_5OH, and other C_{2+} products with Cu mesh and Cu mesh/Nafion.

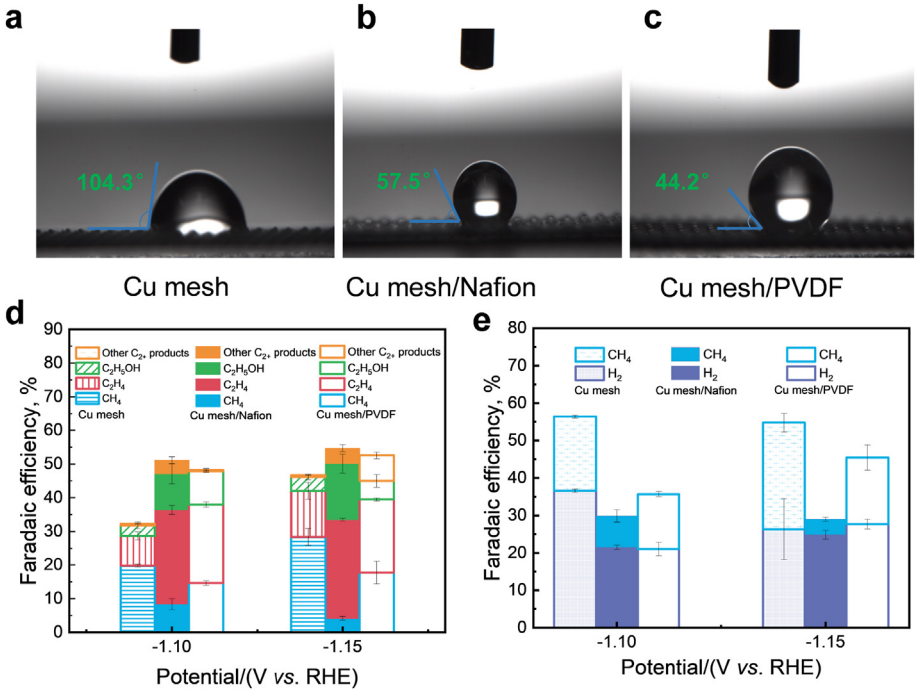

Fig. 3. Hydrophobicity of Cu mesh, Cu mesh/Nafion, and Cu mesh/PVDF and comparison of their CO_2RR performance. (a~c) The contact angle for Cu mesh, Cu mesh/Nafion, and Cu mesh/PVDF, respectively. (d) Faradaic efficiency of CH_4, C_2H_4, C_2H_5OH, and other C_{2+} products with Cu mesh, Cu mesh/Nafion, and Cu mesh/PVDF at potential −1.10 V and −1.15 V *vs.* RHE. (e) Faradaic efficiency of CH_4 and H_2 with Cu mesh, Cu mesh/Nafion, and Cu mesh/PVDF at potential −1.10 V and −1.15 V *vs.* RHE.

to the values on Cu mesh (Fig. S7). More importantly, on the Cu mesh/Nafion electrode, the cathodic partial current density for C_{2+} products (j_{C2+}) achieves a maximum value of −15.2 mA cm^{-2} at −1.25 V *vs.* RHE, which is about 4 times higher than the one of Cu mesh electrode at the same applied potential (Fig. 2a). Meanwhile, the cathodic partial current density for CH_4 (j_{CH4}) is suppressed by 60% from −6.2 mA cm^{-2} to −2.5 mA cm^{-2} at −1.25 V *vs.* RHE after the modification by Nafion.

Fig. 2b shows the FE of CH_4, C_2H_4, C_2H_5OH, and other C_{2+} products on Cu mesh and Cu mesh/Nafion electrodes under different applied potentials. At −1.20 V *vs.* RHE, the total FE of C_{2+} on Cu mesh/Nafion improves to about 56%, but the FE of CH_4 is suppressed to 5%. The FE ratio of the C_{2+} products-to-CH_4 increases from 0.5 on Cu mesh to 11.2 on Cu mesh/Nafion at −1.20 V *vs.* RHE (Tables S3 and S4). This result further demonstrates the enhanced selectivity of multi-carbon products with the modification of Nafion on the Cu mesh electrode.

The stability of Cu mesh/Nafion was also measured for 18 h of electrolysis (Fig. S8). The total geometric current density and FE of C_2H_4 remain stable for 18 h at −1.20 V *vs.* RHE. There is a slight increase in contact angle after 18 h stability testing (Fig. S9). Besides, XPS spectra of Cu 2p and F 1s are similar to the ones of Cu mesh/Nafion after 35 min CO_2 reduction, illustrating that the chemical oxidation state of Cu remains intact after the long-term stability test (Fig. S10).

3.3. *Effect of hydrophobicity of Cu mesh/Nafion electrode on CO_2RR performance*

Cu mesh/Nafion electrode not only has OH^- repulsion but also has hydrophobic properties. To reveal whether the improved performance of the Cu mesh/Nafion electrode is due to hydrophobicity, we modified the Cu mesh electrode with PVDF (Cu mesh/PVDF) with hydrophobicity and no repulsion of OH^- [29,43,44]. The electrode was prepared similarly to Cu mesh/Nafion. A surface morphology with a network of nanospheres is discernible after modification (Fig. S11).

The contact angles of Cu mesh, Cu mesh/Nafion, and Cu mesh/PVDF are 75.7°, 122.5°, and 135.8°, respectively, confirming the hydrophobicity of both Nafion and PVDF (Fig. 3a–c). After CO_2RR, the contact angles slightly decrease, but remain hydrophobic properties, showing persistent hydrophobicity of Cu mesh/Nafion and Cu mesh/PVDF (Fig. S12).

The performance of Cu mesh/PVDF for CO_2RR was evaluated as a comparison under an applied potential of −1.10 V and −1.15 V. As the potential becomes more negative, the j_{total} and j_{CO2RR} increased in all samples (Fig. S13a). The cathodic current density j_{total} and j_{CO2RR} on Cu mesh/PVDF are −12.9 mA cm^{-2} and −9.0 mA cm^{-2}, respectively at −1.15 V *vs.* RHE, which are lower than the ones on Cu mesh/Nafion (j_{total} = −15.0 mA cm^{-2}, j_{CO2RR} = −11.1 mA cm^{-2}) and higher than the ones on Cu mesh (j_{total} = −11.9 mA cm^{-2}, j_{CO2RR} = −8.6 mA cm^{-2}). The ratio of j_{C2+} to j_{CH4} on Cu mesh/PVDF is 1.96 at −1.15 V *vs.* RHE (Fig. S13b), which is less than 1/5 of the ratio on Cu mesh/Nafion (12.2) but higher than the one on Cu mesh (0.64).

Compared to the Cu mesh electrode, the formation of CH_4 on Cu mesh/PVDF is suppressed at the potential −1.10 V and −1.15 V *vs.* RHE (Fig. 3d). The FE of CH_4 at −1.15 V *vs.* RHE decreases from 28.4% on Cu mesh to 17.7% on Cu mesh/PVDF. But this value is still higher than the one on Cu mesh/Nafion (FE_{CH4} = 4.2%). At −1.15 V *vs.* RHE, the FE of C_{2+} products on Cu mesh/PVDF reaches 34.8%, which is higher than the one on Cu mesh (FE_{C2+} = 18.3%) but lower than the one on Cu mesh/Nafion (FE_{C2+} = 50.5%). Fig. 3e further demonstrates that the Cu mesh/Nafion inhibits CH_4 production more effectively than Cu/PVDF. In a word, we can see that the C_{2+} selectivity on Cu mesh/PVDF is lower than that on Cu mesh/Nafion and higher than that on Cu mesh. However, the Cu mesh/PVDF is more hydrophobicity than Cu mesh/Nafion and Cu mesh. Therefore, hydrophobicity is not the main factor in enhancing C–C coupling.

3.4. *Effect of Cu substrate on CO_2RR performance*

To demonstrate the effect of Cu mesh substrate, we also analyze the performance of Cu foil and Cu foam which were modified by Nafion. The surface morphologies of Cu foil and Cu foam electrodes before and after modification are shown in Figs. S14 and S15. Similar features of Cu mesh/Nafion are observed.

The FE of C_{2+} products on Cu foil/Nafion is enhanced to 35.3%, compared to the FE_{C2+} of 26.9% on Cu foil. The FE of CH_4 is suppressed

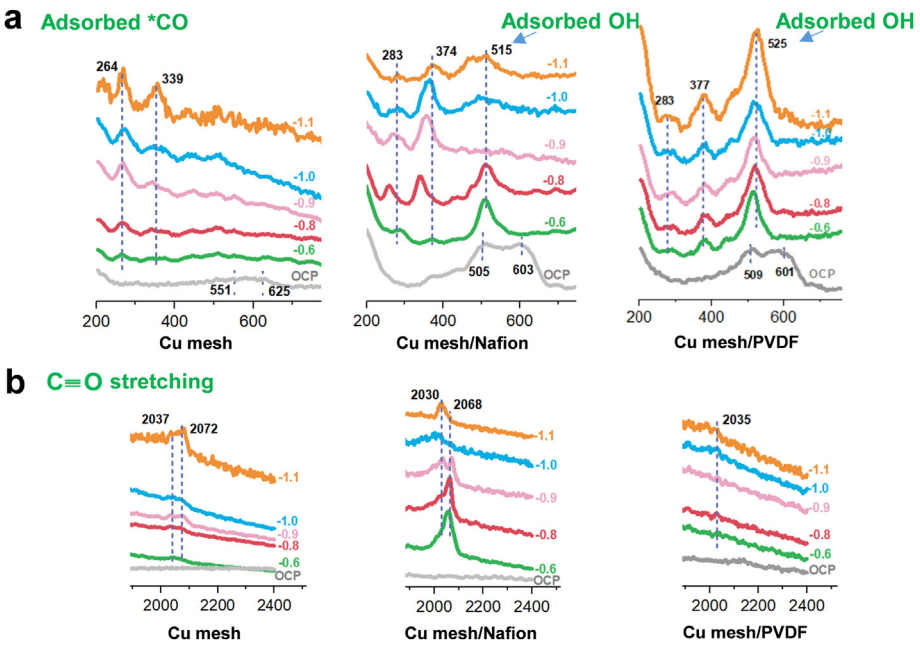

Fig. 4. *Operando* Raman spectroscopy of Cu mesh, Cu mesh/Nafion, and Cu mesh/PVDF catalysts in CO_2-saturated 0.1 M $KHCO_3$ at different potentials. Raman spectroscopy was collected at (a) 200-800 cm^{-1} and (b) 1800-2400 cm^{-1}.

from 28.9% on Cu foil to 12.3% on Cu foil/Nafion at −1.10 V *vs.* RHE (Fig. S16a). The FE ratio of the C_{2+} products-to-CH_4 is 2.9. We also find that the FE_{C2+} of 35% is achieved on Cu foam/Nafion at −1.20 V *vs.* RHE, where the FE_{C2+} is only 11.9% on Cu foam (Fig. S16b). The FE of CH_4 is suppressed effectively from 31.8% on Cu foam to 4.8% on Cu foam/Nafion at −1.20 V *vs.* RHE. And the FE ratio of the C_{2+} products- to-CH_4 is as high as 7.3. Besides, the ratio of the partial current density of j_{C2+} to j_{CH4} on Cu foil/Nafion is 2.88, which is 3.2 times higher than the one Cu foil at −1.10 V *vs.* RHE (Fig. S17a). Compared to Cu foam with j_{C2+} of −3.4 mA cm^{-2} and j_{CH4} of −9.2 mA cm^{-2} at −1.20 V *vs.* RHE, j_{C2+} and j_{CH4} on Cu foam/Nafion are −10.3 and −1.4 mA cm^{-2}, respectively (Fig. S17b). Thus, though the type of Cu substrate has an impact on the overall performance, the effect of Nafion on improving the activity of C–C coupling and suppressing CO protonation to CH_4 appears to be a universal phenomenon regardless of the type of Cu substrate being used.

3.5. The intrinsic catalytic activity of Cu mesh/Nafion

To evaluate the intrinsic catalytic activity, the electrochemically active surface areas (ECSAs) of Cu mesh and Cu mesh/Nafion were measured *via* double-layer capacitance (Fig. S18 and Table S5). The specific current densities are shown in Fig. S19. Cu mesh/Nafion obtains a higher specific current density of j_{total} and j_{CO2RR} than Cu mesh at the potential > −1.10 V *vs.* RHE, demonstrating enhanced activity of CO_2 reduction once Nafion is covered on Cu mesh. As shown in Fig. S19b, the specific current of C_{2+} products is higher than others, which demonstrated that the forming path of C_{2+} products was mainly responsible for increasing the specific current density. In addition, a smaller specific current density of CH_4 with −0.41 mA cm^{-2} is observed on Cu mesh/Nafion while Cu mesh delivers a specific current density of −2.1 mA cm^{-2} for CH_4 production at −1.20 V *vs.* RHE. This further illustrated that the CH_4 was suppressed effectively.

The production rate of CO (TOF_{CO}) is composed of gas ($TOF_{CO(g)}$) and intermediates species to be further reduced to hydrocarbons and alcohols (TOF_{*CO}). The TOF_{CO}, $TOF_{CO(g)}$, and TOF_{*CO} were calculated to further analyze the effect of the Nafion. As shown in Fig. S20, TOF_{*CO} represents the amount of CO that is further reduced to multi-carbon products, and TOF_{CH4} is the CO further reduced to CH_4 product. TOF_{*CO} increases from 1887.5 nmol s^{-1} cm^{-2} on Cu mesh to 7893.9 nmol s^{-1} cm^{-2} on Cu mesh/Nafion at −1.2 V *vs.* RHE, where ΔTOF_{*CO} = 6006.4 nmol s^{-1} cm^{-2}. However, TOF_{CH4} decreased from 2703.6 nmol s^{-1} cm^{-2} on Cu mesh to 531.5 nmol s^{-1} cm^{-2} on Cu mesh/Nafion at the same potential. That is to say, the increased CO production is further reduced to multi-carbon products instead of CH_4.

3.6. Operando Raman spectroscopy of catalysts in CO_2 reduction

Operando Raman spectroscopy was used to identify the relationship of the intermediate CO and OH adsorption on the electrode in CO_2-saturated 0.1 M $KHCO_3$ (Fig. 4). The oxidation of the Cu surface is demonstrated by the peaks at 500-625 cm^{-1} under open-circuit potential (OCP) (Fig. 4a). There are no peaks from 1800 to 2400 cm^{-1} on the three different electrodes under OCP (Fig. 4b).

As shown in Fig. 4a, we found that two bands are presented on Cu mesh, Cu mesh/Nafion, and Cu mesh/PVDF at 260–283 and 339-377 cm^{-1} under negative bias from −0.6 V to −1.1 V. These peaks could be attributed to the restricted rotation of Cu–CO and Cu–CO stretching, respectively [45–48]. In addition, unlike Cu mesh, there is a peak at 515-525 cm^{-1} from −0.6 V to −1.1 V on the Cu mesh/Nafion and Cu mesh/PVDF, which was considered as OH adsorbed [47].

The range from 1800 to 2400 cm^{-1} Raman spectrum in Fig. 4b shows one band on Cu mesh and Cu mesh/Nafion at 2030–2072 cm^{-1} under negative bias from −0.6 V to −1.1 V, which was attributed to C≡O stretching [45–48]. However, there are no peaks on Cu mesh/PVDF at this range. Considering that there is a strong adsorbed OH signal on the Cu mesh/PVDF, we infer that the disappeared peak at 2035 cm^{-1} may be due to more OH occupying the active sites caused by the hydrophobic surface, leading to less CO adsorption [36]. Although OH is adsorbed on Cu mesh/Nafion, the negative background charge of Nafion has a repulsion of OH^- [49], which could reduce part of OH^- near the electrode to maintain the CO adsorption site. There may be other possible reasons, such as the structure, chemical properties, or functional groups of PVDF affecting the adsorption of CO intermediates on the active sites. However, according to this work, the PVDF as a comparative sample was presented to verify the role of hydrophobic properties in selectivity, which will be forming more OH occupying the active sites. Besides, the reported work shows that high local pH can enhance C–C coupling [50, 51]. Due to the hydrophobicity of Cu mesh/PVDF, the higher local pH

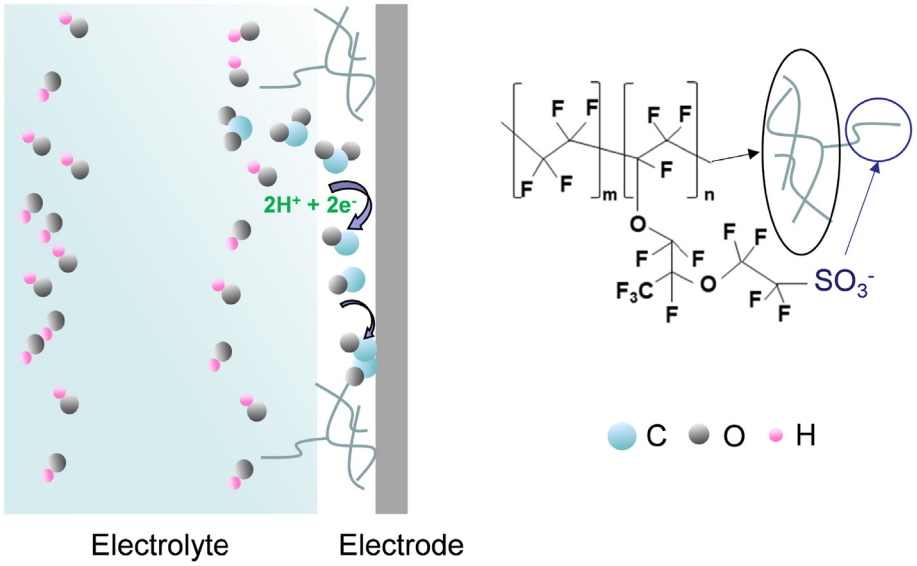

Fig. 5. Schematic illustration of the stabilized CO and local concentration of OH^- on the surface of Cu mesh/Nafion.

will improve the C–C coupling. Therefore, the C_{2+} performance of Cu mesh/PVDF is higher than Cu mesh (Figs. 3 and 4). However, more OH will affect the CO adsorbed on the active sites, leading to lower selectivity than Cu mesh/Nafion (Figs. 3 and 4). As a result, the balance of concentration of OH and CO adsorption is the key to enhancing the selectivity of C_{2+} products.

3.7. The schematic illustration of Cu mesh/Nafion for improved C–C coupling and local OH

The schematic illustration of the local environment near the electrode, C–C coupling on the interface, and the structure of the Nafion are shown in Fig. 5. Cu mesh electrode modified with Nafion, which formed hydrophobic surface with the repulsion of OH^- characteristic. The CO_2 reduction to CO intermediate and C–C coupling were presented on this interface. The Nafion layer with a negative background charge produced a repulsion of OH^-, and then modulated the local concentration of OH^- near the electrode. This modified local environment not only can ensure the CO adsorption on the active sites but also enhance the C–C coupling. At last, these results suppressed the CH_4 forming and improved the selectivity of multi-carbon products.

4. Conclusions

In a word, we designed an electrode with the repulsion of OH^-, which enables optimized CO adsorption and enhanced C–C coupling. The quantitative analysis of FE and partial current density of the products demonstrated the enhanced selectivity of C_{2+} products and the effective suppression of CH_4 evolution. The *operando* Raman spectroscopy was performed to identify the relationship between OH and CO adsorption. Furthermore, different hydrophobic modifiers were employed to demonstrate that the repulsion of OH^- is necessary for improving the performance of CO_2 reduction to multi-carbon products. Besides, the effect of Nafion on improved C–C coupling is demonstrated to be universal regardless of the type of Cu electrode being used. This work provides a strategy of electrode design for effective CO_2 reduction to multi-carbon products.

Author contributions

Q. X. Z. and D. R. contributed equally to this work.
X. D. Z. supervised the project. Q. X. Z. designed and executed the experiments. D. R. and J. G. conducted the *operando* Raman step and data processing. J. S. L. and X. D. Z. provided the experiment platform. Z. K. W., J. W., S. J. P., and M. J. W aided in the course of the experiment. M. G. and Y. Z. provided constructive advice. Q. X. Z., D. R., X. D. Z., and M. G. contributed to the writing and revising of the manuscript. All authors discussed the results and contributed to the manuscript.

Declaration of competing interests

The authors declare that they have no known competing financial interests or personal relationships that could have appeared to influence the work reported in this paper.

Acknowledgments

This work was supported by the following projects: INTERNATIONAL COOPERATION Projects of the Ministry of Science and Technology (2014DFE60170), the Strategic Japanese–Swiss Science and Technology Program from the Swiss National Science Foundation (project No. IZJSZ2_180176), the Sino-Swiss Science and Technology Cooperation (SSSTC) 2016 project from the Swiss National Science Foundation (project No. IZLCZ2_170294), the National Natural Science Foundation of China (Grant No. 61674084), the Overseas Expertise Introduction Project for Discipline Innovation of Higher Education of China (Grant No. B16027), Tianjin Science and Technology Project (Grant No. 18ZXJMTG00220), and the Fundamental Research Fund for the Central Universities of China.

Appendix A. Supplementary data

Supplementary data to this article can be found online at https://doi.org/10.1016/j.gce.2022.07.007.

References

[1] D. Gao, R.M. Aran-Ais, H.S. Jeon, B.R. Cuenya, Rational catalyst and electrolyte design for CO_2 electroreduction towards multicarbon products, Nat. Catal. 2 (2019) 198–210.
[2] Y.Y. Birdja, E. Perez-Gallent, M.C. Figueiredo, A.J. Gottle, F. Calle-Vallejo, M.T. Koper, Advances and challenges in understanding the electrocatalytic conversion of carbon dioxide to fuels, Nat. Energy 4 (2019) 732–745.
[3] S. Nitopi, E. Bertheussen, S.B. Scott, X. Liu, A.K. Engstfeld, S. Horch, B. Seger, I.E.L. Stephens, K. Chan, C. Hahn, J.K. Nørskov, T.F. Jaramillo, I. Chorkendorff, Progress and perspectives of electrochemical CO_2 reduction on copper in aqueous electrolyte, Chem. Rev. 119 (2019) 7610–7672.

[4] G. Wang, J. Chen, Y. Ding, P. Cai, L. Yi, Y. Li, C. Tu, Y. Hou, Z. Wen, L. Dai, Electrocatalysis for CO_2 conversion: from fundamentals to value-added products, Chem. Soc. Rev. 50 (2021) 4993–5061.
[5] Y. Zhang, S. Guo, X. Zhang, A. Bond, J. Zhang, Cu_2O nanocubes with mixed oxidation–state facets for (photo)catalytic hydrogenation of carbon dioxide, Nano Today 31 (2020) 100835.
[6] Z. Wu, F. Gao, M. Gao, Regulating the oxidation state of nanomaterials for electrocatalytic CO_2 reduction, Energy Environ. Sci. 14 (2021) 1121–1139.
[7] E.E. Benson, C.P. Kubiak, A.J. Sathrum, J.M. Smieja, Electrocatalytic and homogeneous approaches to conversion of CO_2 to liquid fuels, Chem. Soc. Rev. 38 (2009) 89–99.
[8] Y. Hori, K. Kikuchi, S. Suzuki, Production of CO and CH_4 in electrochemical reduction of CO_2 at metal electrodes in aqueous in aqueous hydrogencarbonate solution, Chem. Lett. 11 (1985) 1695–1698.
[9] Y. Wang, H. Shen, K. Livi, D. Raciti, H. Zong, J. Gregg, M. Onadeko, Y. Wan, A. Watson, C. Wang, Copper nanocubes for CO_2 reduction in gas diffusion electrodes, Nano Lett. 19 (2019) 8461–8468.
[10] K. Jiang, R. Sandberg, A. Akey, X. Liu, D. Bell, J. Nørskov, K. Chan, H. Wang, Metal ion cycling of Cu foil for selective C–C coupling in electrochemical CO_2 reduction, Nat. Catal. 1 (2018) 111–119.
[11] R. Mariano, K. McKelvey, H. White, M. Kanan, Selective increase in CO_2 electroreduction activity at grain-boundary surface terminations, Science 358 (2017) 1187–1192.
[12] X. Feng, K. Jiang, S. Fan, M. Kanan, A direct grain-boundary-activity correlation for CO electroreduction on Cu nanoparticles, ACS Cent. Sci. 2 (2016) 169–174.
[13] Z. Chen, T. Wang, B. Liu, D. Cheng, C. Hu, G. Zhang, W. Zhu, H. Wang, Z. Zhao, J. Gong, Grain-boundary-rich copper for efficient solar-driven electrochemical CO_2 reduction to ethylene and ethanol, J. Am. Chem. Soc. 142 (2020) 6878–6883.
[14] L. Li, D. Ma, F. Qi, W. Chen, S. Huang, Bi nanoparticles/Bi_2O_3 nanosheets with abundant grain boundaries for efficient electrocatalytic CO_2 reduction, Electrochim. Acta 298 (2019) 580–586.
[15] L. Wang, S. Nitopi, A. Wong, J. Snider, A. Nielander, C. Morales-Guio, M. Orazov, D. Higgins, C. Hahn, T. Jaramillo, Electrochemically converting carbon monoxide to liquid fuels by directing selectivity with electrode surface area, Nat. Catal. 2 (2019) 702–708.
[16] Y. Zhao, X. Chang, A. Malkani, X. Yang, L. Thompson, F. Jiao, B. Xu, Speciation of Cu surfaces during the electrochemical CO reduction reaction, J. Am. Chem. Soc. 142 (2020) 9735–9743.
[17] J. Lv, M. Jouny, W. Luc, W. Zhu, J. Zhu, F. Jiao, A highly porous copper electrocatalyst for carbon dioxide reduction, Adv. Mater. 30 (2018) 1803111.
[18] T. Hoang, S. Verma, S. Ma, T. Fister, J. Timoshenko, A. Frenkel, P. Kenis, A. Gewirth, Nanoporous copper-silver alloys by additive-controlled electrodeposition for the selective electroreduction of CO_2 to ethylene and ethanol, J. Am. Chem. Soc. 140 (2018) 5791–5797.
[19] X. Chen, D. Henckel, U. Nwabara, Y. Li, A. Frenkel, T. Fister, P. Kenis, A. Gewirth, Controlling speciation during CO_2 reduction on Cu-alloy electrodes, ACS Catal. 10 (2020) 672–682.
[20] X. Liu, P. Schlexer, J. Xiao, Y. Ji, L. Wang, R. Sandberg, M. Tang, K. Brown, H. Peng, S. Ringe, C. Hahn, T. Jaramillo, J. Nørskov, K. Chan, PH effects on the electrochemical reduction of CO_2 towards C_2 products on stepped copper, Nat. Commun. 10 (2019) 32.
[21] A. Varela, M. Kroschel, N. Leonard, W. Ju, J. Steinberg, A. Bagger, J. Rossmeisl, P. Strasser, PH effects on the selectivity of the electrocatalytic CO_2 reduction on graphene embedded Fe−N−C motifs: bridging concepts between molecular homogeneous and solid state heterogeneous catalysis, ACS Energy Lett. 3 (2018) 812–817.
[22] G. Larrazábal, T. Shinagawa, A. Martín, J. Pérez-Ramírez, Microfabricated electrodes unravel the role of interfaces in multicomponent copper-based CO_2 reduction catalysts, Nat. Commun. 9 (2018) 1477.
[23] N. Nesbitt, T. Burdyny, H. Simonson, D. Salvatore, D. Bohra, R. Kas, W. Smith, Liquid–solid boundaries dominate activity of CO_2 reduction on gas-diffusion electrodes, ACS Catal. 10 (2020) 14093–14106.
[24] A. Vojvodic, J.K. Nørskov, New design paradigm for heterogeneous catalysts, Natl. Sci. Rev. 2 (2015) 140–143.
[25] A.A. Peterson, J.K. Nørskov, Activity descriptors for CO_2 electroreduction to methane on transition-metal catalysts, J. Phys. Chem. Lett. 3 (2012) 251–258.
[26] D. Wakerley, S. Lamaison, F. Ozanam, N. Menguy, D. Mercier, P. Marcus, M. Fontecave, V. Mougel, Bio-inspired hydrophobicity promotes CO_2 reduction on a Cu surface, Nat. Mater. 18 (2019) 1222–1227.
[27] Z. Niu, F. Gao, X. Zhang, P. Yang, R. Liu, L. Chi, Z. Wu, S. Qin, X. Yu, M. Gao, Hierarchical copper with inherent hydrophobicity mitigates electrode flooding for high-rate CO_2 electroreduction to multicarbon products, J. Am. Chem. Soc. 143 (2021) 8011–8021.
[28] Z. Xing, L. Hu, D. Ripatti, X. Hu, X. Feng, Enhancing carbon dioxide gas-diffusion electrolysis by creating a hydrophobic catalyst microenvironment, Nat. Commun. 12 (2021) 136.
[29] H. Liang, S. Zhao, X. Hu, M. Ceccato, T. Skrydstrup, K. Daasbjerg, Hydrophobic copper interfaces boost electroreduction of carbon dioxide to ethylene in water, ACS Catal. 11 (2021) 958–966.
[30] Y. Sa, C. Lee, S. Lee, J. Na, U. Lee, Y. Hwang, Catalyst–electrolyte interface chemistry for electrochemical CO_2 reduction, Chem. Soc. Rev. 49 (2020) 6632–6665.
[31] Y. Fang, J. Flake, Electrochemical reduction of CO_2 at functionalized au electrodes, J. Am. Chem. Soc. 139 (2017) 3399–3405.
[32] C. Yang, S. Li, Z. Zhang, H. Wang, H. Liu, F. Jiao, Z. Guo, X. Zhang, W. Hu, Organic–inorganic hybrid nanomaterials for electrocatalytic CO_2 reduction, Small 16 (2020) 2001847.
[33] Y. Wu, S. Cao, J. Hou, Z. Li, B. Zhang, P. Zhai, Y. Zhang, L. Sun, CO_2 reduction: rational design of nanocatalysts with nonmetal species modification for electrochemical CO_2 reduction, Adv. Energy Mater. 10 (2020) 2000588.
[34] Y. Zhang, S. Guo, X. Zhang, A. Bond, J. Zhang, Mechanistic understanding of the electrocatalytic CO_2 reduction reaction – new developments based on advanced instrumental techniques, Nano Today 31 (2020) 100835.
[35] C.-T. Dinh, T. Burdyny, M.G. Kibria, A. Seifitokaldani, C.M. Gabardo, F.P. García de Arquer, A. Kiani, J.P. Edwards, P. De Luna, O.S. Bushuyev, C. Zou, CO_2 electroreduction to ethylene *via* hydroxide-mediated copper catalysis at an abrupt interface, Science 360 (2018) 783–787.
[36] T. Todorova, M.W. Schreiber, M. Fontecave, Mechanistic understanding of CO_2 reduction reaction (CO_2RR) toward multicarbon products by heterogeneous copper-based catalysts, ACS Catal. 10 (2020) 1754–1768.
[37] J. Weber, P. Janda, L. Kavan, A. Jegorov, Electrochemical, IR and XPS study of Nafion films prepared from hexamethylphosphortriamide solution, J. Electroanal. Chem. Interfacial Electrochem. 1 (1986) 81–92.
[38] S. Poulston, P.M. Parlett, P. Stone, M. Bowker, Surface oxidation and reduction of CuO and Cu_2O studied using XPS and XAES, Surf. Interface Anal. 24 (1996) 811–820.
[39] M. Deo, S. Mujawar, O. Game, A. Yengantiwar, A. Banpurkar, S. Kulkarni, J. Jog, S. Ogale, Strong photo-response in a flip-chip nanowire p-Cu_2O/n-ZnO junction, Nanoscale 3 (2011) 4706–4712.
[40] A. Dutta, M. Rahaman, N.C. Luedi, M. Mohos, P. Broekmann, Morphology matters: tuning the product distribution of CO_2 electroreduction on oxide-derived Cu foam catalysts, ACS Catal. 6 (2016) 3804–3814.
[41] J. Zeng, K. Bejtka, W. Ju, M. Castellino, A. Chiodoni, A. Sacco, M. Farkhondehfal, S. Hernández, D. Rentsch, C. Battaglia, C. Pirri, Advanced Cu-Sn foam for selectively converting CO_2 to CO in aqueous solution, Appl. Catal., B 236 (2018) 475–482.
[42] J. Gao, H. Zhang, X. Guo, J. Luo, S. Zakeeruddin, D. Ren, M. Grätzel, Selective C-C coupling in carbon dioxide electroreduction *via* efficient spillover of intermediates as supported by *operando* Raman spectroscopy, J. Am. Chem. Soc. 141 (2019) 18704–18714.
[43] J. Lee, S. Kattel, Z. Xie, B. Tackett, J. Wang, C. Liu, J. Chen, Understanding the role of functional groups in polymeric binder for electrochemical carbon dioxide reduction on gold nanoparticles, Adv. Funct. Mater. 28 (2018) 1804762.
[44] E. Andrews, S. Katla, C. Kumar, M. Patterson, P. Sprunger, J. Flake, Electrocatalytic reduction of CO_2 at Au nanoparticle electrodes: effects of interfacial chemistry on reduction behavior, J. Electrochem. Soc. 162 (2015) F1373–F1378.
[45] D. Ren, J. Gao, L. Pan, Z. Wang, J. Luo, S.M. Zakeeruddin, A. Hagfeldt, M. Grätzel, Atomic layer deposition of ZnO on CuO enables selective and efficient electroreduction of carbon dioxide to liquid fuels, Angew. Chem. Int. Ed. 58 (2019) 15036.
[46] I. Oda, H. Ogasawara, M. Ito, Carbon monoxide adsorption on copper and silver electrodes during carbon dioxide electroreduction studied by infrared reflection absorption spectroscopy and surface-enhanced Raman spectroscopy, Langmuir 12 (1996) 1094–1097.
[47] Y. Yang, S. Ajmal, Y. Feng, K. Li, X. Zheng, L. Zhang, Insight into the formation and transfer process of first intermediate of CO_2 reduction over Ag-decorated dendritic Cu, Chem. Eur. J. 26 (2020) 4080–4089.
[48] Y. Yang, L. Ohnoutek, S. Ajmal, X. Zheng, Y. Feng, K. Li, T. Wang, Y. Deng, Y. Liu, D.K. Xu, V. Valev, L. Zhang, "Hot edges" in an inverse opal structure enable efficient CO_2 electrochemical reduction and sensitive *in situ* Raman characterization, J. Mater. Chem. A 7 (2019) 11836–11846.
[49] C. Kim, J.C. Bui, X. Luo, J.K. Cooper, A. Kusoglu, A.Z. Weber, A.T. Bell, Tailored catalyst microenvironments for CO_2 electroreduction to multicarbon products on copper using bilayer ionomer coatings, Nat. Energy 6 (2021) 1026–1034.
[50] M. Jouny, M. Luc, F. Jiao, High-rate electroreduction of carbon monoxide to multi-carbon products, Nat. Catal. 1 (2018) 748–755.
[51] H. Xiao, T. Cheng, W.A. Goddard, R. Sundararaman, Mechanistic explanation of the pH dependence and onset potentials for hydrocarbon products from electrochemical reduction of CO on Cu (111), J. Am. Chem. Soc. 138 (2016) 483–486.